Department of Applied Physics

Point defects in nanocrystals and semiconductors studied with positron annihilation spectroscopy

Jiri Kujala

Aalto University

DOCTORAL DISSERTATIONS

Aalto University publication series
DOCTORAL DISSERTATIONS 223/2016

Point defects in nanocrystals and semiconductors studied with positron annihilation spectroscopy

Jiri Kujala

A doctoral dissertation completed for the degree of Doctor of Science (Technology) to be defended, with the permission of the Aalto University School of Science, at a public examination held at the lecture hall E of the school on 4 October 2016 at 13.

Aalto University
School of Science
Department of Applied Physics
Antimatter and Nuclear Engineering

Supervising professor
Prof. Filip Tuomisto, Aalto University, Finland

Thesis advisor
Ph.D. Jonatan Slotte, Aalto University, Finland

Preliminary examiners
Prof. André Vantomme, University of Leuven, Belgium
Prof. Timo Sajavaara, University of Jyväskylä, Finland

Opponent
Prof. Stephan Eijt, Delft University of Technology, Netherlands

Aalto University publication series
DOCTORAL DISSERTATIONS 223/2016

ISBN 978-952-60-7092-6 (printed)
ISBN 978-952-60-7089-6 (pdf)
ISSN-L 1799-4934
ISSN 1799-4934 (printed)
ISSN 1799-4942 (pdf)
http://urn.fi/URN:ISBN:978-952-60-7089-6

Unigrafia Oy
Helsinki 2016

Finland

441 697
Printed matter

Author
Jiri Kujala

Name of the doctoral dissertation
Point defects in nanocrystals and semiconductors studied with positron annihilation spectroscopy

Publisher School of Science

Unit Department of Applied Physics

Series Aalto University publication series DOCTORAL DISSERTATIONS 223/2016

Field of research Engineering Physics

Manuscript submitted 13 October 2016 **Date of the defence** 4 November 2016

Permission to publish granted (date) 13 October 2016 **Language** English

☐ **Monograph** ☒ **Article dissertation** ☐ **Essay dissertation**

Abstract

The optical properties of bulk silicon are notoriously poor due to its indirect band gap. By reducing the crystal size to the nanometer scale, the band gap becomes direct. This leads to a considerable improvement in the optical properties of the crystal. Silicon nanocrystals embedded in silica are studied with positron annihilation and photoluminescence spectroscopies. The results indicate that the interface between the nanocrystal and the surrounding silica lattice acts as a strong trap for positrons. The lattice defects located at the interface were noted to passivate after annealing performed in the hydrogen gas.

In this work, strongly phosphorous doped silicon samples are studied. A lattice strain is induced in highly phosphorous doped silicon due to the formation of defect structures. According to earlier reports the cause for the strain are Si_3P_4 clusters. Calculations based on density functional theory indicates that the formation enthalpy of these clusters is higher than the thermal energy available during the growth of the sample. Unlike Si_3P_4, the formation enthalpy of V-P_n complexes is negative, which would indicate that these structures are spontaneously formed in the growth process. The theoretical calculations are consistent with the Doppler broadening results, which state that the dominating lattice defect is a monovacancy decorated with several impurity atoms.

Thanks to its lattice constant, GaSb is a suitable substrate material for various group III-V semiconductors whose band gaps cover a wide energy range. Undoped GaSb is *p*-type irrespective of its growth method. In this work, undoped and tellurium doped GaSb are studied. Doppler broadening and lifetime spectroscopy measurements show that the dominating vacancy defect is gallium vacancy. However, the primary cause, for the undoped GaSb being *p*-type, is the ion-type defect in which a Sb sublattice site is occupied by Ga atom.

Highly arsenic, phosphorous and antimony doped germanium samples are studied with the help of Doppler broadening and lifetime measurements. The results indicate, that the dominating defect type in all samples is a complex consisting of a monovacancy and three impurity atoms. In the case of arsenic and phosphorous doped germanium samples, the positron trapping is in saturation or in a saturation-like state, whereas in antimony doped germanium sample only a fraction of the positrons are trapped to complexes prior to annihilation.

Keywords semiconductors, nanocrystals, vacancies, complexes, positron spectroscopy

ISBN (printed) 978-952-60-7092-6 **ISBN (pdf)** 978-952-60-7089-6

ISSN-L 1799-4934 **ISSN (printed)** 1799-4934 **ISSN (pdf)** 1799-4942

Location of publisher Helsinki **Location of printing** Helsinki **Year** 2016

Pages 98 **urn** http://urn.fi/URN:ISBN:978-952-60-7089-6

Tekijä
Jiri Kujala

Väitöskirjan nimi
Pistevirheiden tutkiminen nanokiteissä ja puolijohteissa positroniannihilaatiospektroskopialla

Julkaisija Perustieteiden korkeakoulu

Yksikkö Teknillisen fysiikan laitos

Sarja Aalto University publication series DOCTORAL DISSERTATIONS 223/2016

Tutkimusala Teknillinen fysiikka

Käsikirjoituksen pvm 13.10.2016 **Väitöspäivä** 04.11.2016

Julkaisuluvan myöntämispäivä 13.10.2016 **Kieli** Englanti

☐ **Monografia** ☒ **Artikkeliväitöskirja** ☐ **Esseeväitöskirja**

Tiivistelmä

Bulkkipiin optiset ominaisuudet ovat tunnetusti huonoja johtuen sen epäsuorasta energia-aukosta. Pienentämällä kiteen kokoa nanometriluokkaan, jolloin sen energia-aukosta tulee suora, nähdään huomattava parannus optisissa ominaisuuksissa. Piioksidiin upotettuja piinanokiteitä on tutkittu positroniannihilaatio- ja fotoluminesenssispektroskopioiden avulla. Tuloksista voidaan todeta, että rajapinta piinanokiteen ja ympäröivän piioksidihilan välissä toimii voimakkaana loukkuna positroneille. Rajapinnassa sijaitsevien hilavirheiden todettiin passivoituvan typpivety-kaasussa tehdyn toivutuksen myötä.

Voimakkaasti fosforilla seostettuun piihilaan aiheutuu venymä, joka johtuu piihin muodostuvista hilavirherakenteista. Aikaisempien tutkimusten perusteella venymän syynä on pidetty Si_3P_4-ryppäitä. Tiheysfunktionaaliteoriaan pohjautuvat elektronitiheyslaskut kuitenkin osoittavat, että tällaisten ryppäiden muodostumisentalpia on suurempi kuin näytteen kasvatuksen aikana käytettävissä oleva terminen energia. Sen sijaan, V-P_n-tyyppisillä komplekseilla muodostumisentalpia on negatiivinen, joka viittaisi siihen, että tällaisia rakenteita syntyy spontaanisti kasvatuksen aikana. Teoreettiset laskut ovat sopusoinnussa Doppler-levenemätulosten kanssa joiden mukaan hallitsevin hilavirhe on monovakanssi, jonka ympärillä on useampi epäpuhtausatomi.

GaSb on hilavakionsa ansiosta sopiva alustamateriaali useammalle ryhmän III-V puolijohteelle, joiden energia-aukot kattavat laajan energiavälin. Seostamaton GaSb on *p*-tyyppistä riippumatta sen kasvatustavasta. Tässä työssä on tutkittu seostamatonta ja telluurilla seostettua GaSb näytettä. Doppler-levenemä- ja elinaikamittausten perusteella hallitsevin vakanssityyppinen hilavirhe on galliumvakanssi, mutta pääasiallinen syy sille, että seostamaton GaSb on *p*-tyyppistä, on ioni-tyyppinen virhe, jossa Ga-atomi on Sb-atomin hilapaikalla.

Voimakkaasti arseenilla, fosforilla ja antimonilla seostettuja germaniumnäytteitä on tutkittu Doppler-levenemä- ja elinaikamittausten avulla. Tuloksista nähdään, että hallitsevin virhetyyppi kaikissa näytteissä on kompleksi, joka koostuu vakanssista ja kolmesta epäpuhtausatomista. Arseenilla ja fosforilla seostettujen germaniumnäytteiden tapauksessa positroniannihilaatio on saturaatiossa tai saturaation tyyppisessä tilassa, kun taas antimonilla seostetussa germaniumnäytteessä vain osa positroneista loukkuuntuu komplekseihin ennen annihilaatiota.

Avainsanat puolijohteet, nanokiteet, vakanssit, kompleksit, positronispektroskopia

ISBN (painettu) 978-952-60-7092-6 **ISBN (pdf)** 978-952-60-7089-6

ISSN-L 1799-4934 **ISSN (painettu)** 1799-4934 **ISSN (pdf)** 1799-4942

Julkaisupaikka Helsinki **Painopaikka** Helsinki **Vuosi** 2016

Sivumäärä 98 **urn** http://urn.fi/URN:ISBN:978-952-60-7089-6

Preface

This thesis was prepared in the Antimatter and Nuclear Engineering group in the Department of Applied Physics at the Aalto University School of Science during the years 2011-2016.

I wish to thank Prof. Filip Tuomisto for giving me the opportunity to work in this group. I also want to thank Ph.D. Jonatan Slotte who has been instructing and supporting me in this thesis project.

I want to thank Doc. Ilja Makkonen for introducing me the computational part of physics and Doc. Klaus Rytsölä for his help in solving numerous technical problems that the group have faced. Also, very big thank goes to the group members, both the former and current for the pleasant working atmosphere. Special thanks goes to my friends who keep reminding me, in their own funny and weird way, to take my eyes off the computer screen every now and then!

I also want to thank my parents and my siblings for supporting me in my decision to start doctoral studies. Finally, I want to thank my dear wife Merve for both encouraging me to move forward when I faced an upward hill and reminding me to slow down when the way down was too steep.

Espoo, October 13, 2016,

Jiri Kujala

Contents

List of Publications

This thesis consists of an overview and of the following publications which are referred to in the text by their Roman numerals.

I S. Kilpeläinen, J. Kujala, F. Tuomisto, J. Slotte, Y-W. Lu and A. Nylandsted Larsen. Si nanoparticle interfaces in Si/SiO_2 solar cell materials. *Journal of Applied Physics*, **114**, 16, 164316, October 2013.

II J. Kujala, J. Slotte, F. Tuomisto, D. Hiller and M. Zacharias. Si nanocrystals and nanocrystal interfaces studied by positron annihilation. *Journal of Applied Physics*, **120**, 14, 145302, October 2016.

III S K. Dhayalan, J. Kujala, J. Slotte, G. Pourtois, E. Simoen, E. Rosseel, A. Hikavyy, Y. Shimura, S. Iacovo, A. Stesmans, R. Loo and W. Vandervorst. On the manifestation of phosphorus-vacancy complexes in epitaxial Si:P films. *Applied Physics Letters*, **108**, 8, 082106, February 2016.

IV J. Kujala, T. Südkampand, J. Slotte, I. Makkonen, F. Tuomisto, H. Bracht. Vacancy-donor complexes in highly n-type Ge doped with As, P and Sb. *Journal of Physics: Condensed Matter*, **28**, 33, 335801, June 2016.

V J. Kujala, N. Segercrantz, F. Tuomisto and J. Slotte. Native point defects in GaSb. *Journal of Applied Physics*, **116**, 14, 143508, October 2014.

Author's Contribution

Publication I: "Si nanoparticle interfaces in Si/SiO_2 solar cell materials"

The author performed part of the Doppler broadening experiments, analyzed the experimental data and participated in writing of the manuscript.

Publication II: "Si nanocrystals and nanocrystal interfaces studied by positron annihilation"

The author performed the positron experiments. He analyzed the PAS data and wrote the first draft of the manuscript.

Publication III: "On the manifestation of phosphorus-vacancy complexes in epitaxial Si:P films"

The author performed the Doppler broadening experiments, analyzed the experimental data and participated in writing of the manuscript.

Publication IV: "Vacancy-donor complexes in highly n-type Ge doped with As, P and Sb"

The author performed the positron experiments and theoretical calculations. He analyzed the experimental and computational data and wrote the first draft of the manuscript.

Publication V: "Native point defects in GaSb"

The author performed the positron experiments. He analyzed the experimental data and wrote the first draft of the manuscript.

1. Introduction

Semiconductors have had an increasing role in society ever since their discovery. The research on semiconducting materials, started in the first decades of the 20th century, have been fruitful with researchers striving towards smaller and more powerful devices. Today, mobile phones, laptops, tablets and many other types of devices are available thanks to the development of microprocessors. The growing number of transistors placed on a small circuit board sets a growing demand on control of the fabrication process. A very good knowledge on the properties of the semiconductor material is essential in order to solve the challenges faced by the researchers today and in the future. These include the understanding of the mechanical, optical and electrical properties of the semiconductor as well as having knowledge of its thermal and chemical stability.

The mechanical and electrical properties of the semiconductors depends largely on the crystal structure. Defects cause discontinuities in the ordered arrangement of the atoms. These discontinuities can be anything from a single missing atom to voids, cracks or dislocations. Such disturbances in the atomic order have significant effects on the material properties. For example, doping GaSb with N results in a strong modification of the conduction band. [1–4]. The doping of Si with P or C atoms introduces strain in the lattice which in turn has a beneficial effect on the mobility of the charge carriers. [5–7]

In this thesis defect structures are studied with positron annihilation spectroscopy (PAS), which is a nondestructive method for studying the size, concentration, charge state and chemical surroundings of vacancies. Two different PAS techniques were used: Doppler broadening and positron lifetime spectroscopy. In both of these techniques the annihilation radiation emitted in the annihilation of the positron and the electron is measured. Modeling of defect structures was done with density func-

tional theory (DFT) calculations. DFT can be used to calculate various positron related parameters for different defect structures, $e.g.$ positron lifetime and electron-positron momentum distributions.

The first two publications in this thesis deal with Si nanocrystals (SiNC) embedded in SiO_2. The low-toxicity, unique optical properties and abundance of Si, makes these nanostructures an interesting candidate for $e.g.$ biomarking, light emitting diodes (LEDs) and sensing materials. The photon multiplication effect and the possibility to adjust the absorption edge of the SiNC are properties that could be useful in solar cell devices. Doppler broadening spectroscopy and photoluminescene (PL) were used for these studies. The results indicate that the interface between the nanocrystal (NC) and the surrounding matrix acts as a strong trap for positrons. Heat treatment in a dilute H_2 atmosphere was shown to passivate the dangling bond defects at the nanoparticle-matrix interface.

The third publication focuses on epitaxially grown Si:P films. Si:P films with a high P concentration ([P]$>1\times10^{21}$cm^{-3}) is suitable for source-drain stressors in n-FinFETs [6, 7]. It has been suggested that the cause for the strain in Si:P is due to local Si_3P_4 clusters which do not contribute to the conductivity. [8]. However, the existence of such local clusters has not been proved neither experimentally nor theoretically. The calculated formation enthalpy for Si_3P_4 cluster is too high to be overcome by the growth temperature of the samples whereas the negative enthalpy of vacancy-phosphorous complexes (V_{1-2}-P_n) suggested that these complexes could be present in the Si:P lattice. PAS measurements revealed that the dominating defect in the as-grown layers is most likely a V-P_n complex. Although the positron trapping to divacancy-sized complexes could not be observed, their presence in the lattice was not ruled out.

The fourth publication deals with Czochralski-grown Ge samples. The high charge carrier mobilities of Ge makes this material an important candidate for various high performance components. Samples were doped with high concentrations of As, P and Sb ($\approx10^{19}$cm^{-3}). PAS measurements revealed that the dominating trap type in all samples was a complex consisting of a vacancy and three donor atoms. In the case of As and P doped Ge all the positrons get trapped to complex centers, whereas in the Sb doped Ge a large fraction of positrons do not get trapped to complexes prior to annihilation.

In the fifth publication the native point defects in bulk GaSb is investigated with PAS. GaSb can be lattice matched with III-V compounds to

form a substrate material for various optical communication devices. Undoped GaSb is always p-type irrespective of its growth method. By utilizing Doppler broadening and positron lifetime spectroscopies it is revealed that while the dominating vacancy defect in GaSb is the gallium vacancy (V_{Ga}), the major cause for the p-type conductivity stems from the gallium antisite (Ga_{Sb}) defects.

2. Defects in semiconductors

Electric conductivity of semiconductors sets them somewhere between an insulator and a metal. Looking at semiconductors from a theoretical standpoint, their quite complex band structure can be simplified to consist only of a conduction band and a valence band. At 0 K the valence band of the intrinsic semiconductor is fully occupied and the conduction band is empty. Thus, the semiconductor is insulating. Increasing the temperature of the sample increases the thermal energy in the lattice and consequently some of the electrons are excited to the conduction band, thus forming electron-hole pairs, $i.e.$ excitons. Intrinsic semiconductors are not the most optimal materials to work with, thus dopant atoms are routinely used for modifying the properties of the semiconductor. Addition of impurities can change the conduction properties of the semiconductor by $e.g.$ modifying the gap width or introduce additional states within the gap. p-type doping can be performed by an addition of elements from group III in the periodic table to a material consisting of atoms that have four valence electrons ($e.g.$ Si). Conversely, n-doping in Si can be achieved by introducing dopant atoms with five valence electrons in their outermost shell into the lattice.

2.1 Point defects in elemental semiconductors

A point defect is created when an atom is removed from its lattice site or is moved to an irregular place in the lattice structure. Point defects can be categorized into four subgroups: 1) A defect where an additional atom is at the off-lattice site between the lattice atoms is called an interstitial defect. An interstitial atom can either be from the host lattice (self-interstitial) or an impurity (impurity interstitial). 2) A substitutional impurity atom is an atom of different species than those in the host lattice that occupies

one of the lattice sites. 3) Vacancies are lattice sites where atoms are simply missing. 4) Antisite defects can be observed in compounds where an atom from sublattice A takes a lattice position in sublattice B. Point defects can also form larger vacancy structures, $e.g.$ divacancies, vacancy-impurity complexes, larger clusters or voids.

The electrical properties of a semiconductor can be changed by point defects. Introduction of these defects can add additional energy levels in the band gap of a semiconductor. They can also act as compensating centers for donors and acceptors, by reducing the carrier concentration of the semiconductor, which in turn can degrade the performance of a device. Defect levels are usually denoted in the band gap by the charge transition level associated with the defect. For example singly and doubly negatively charged acceptor levels are denoted by (1-/0) and (2-/1-) respectively. The charge state of the defect is determined by the position of the Fermi level. If the Fermi level moves up in the band gap, $e.g.$ by doping or by a change in temperature, vacancies become more negative. Conversely when the Fermi level approaches the valence band vacancies become more positive.

2.2 Silicon and Germanium

Si as an elemental semiconductor has always gathered much more attention than Ge in the electronic industry. Si has some benefits compared to Ge such as a larger band gap, a stable oxide and a very low surface state density [9]. This makes silicon a much more preferable material to be used in many applications. The strain induced by Ge when alloyed with Si and the much higher charge carrier mobility of Ge were some of the factors that led to the invention of strained $Si_{1-x}Ge_x$ heterostructures which are now used in modern transistors [10–12]. Furthermore, transistors built entirely out of Ge could allow for the fabrication of even faster components [13]. In addition to advancements in conventional semiconductor technology, research on nanoscale devices has taken leaps in recent years paving way for new Ge-based applications such as hetero-bipolar transistors, high-mobility complementary metal-oxide-semiconductor devices and mid-infrared photodetectors [14]. Due to the high research interest towards Si, the study of the material properties of Ge has been limited, hence studies on defects such as vacancies and vacancy-impurity complexes are scarce. In Publ. IV highly doped Ge is studied with PAS. High doping (10^9 cm^{-3}) for these unique samples is achieved via diffusion.

The E-center, a vacancy-donor-pair (V-D), is one of the most studied defect types in elemental semiconductors. [15–20]. Among the reasons for the high interest to study this defect are its role in charge carrier compensation and dopant diffusion processes. [21] Understanding the basic properties of the E-centers, such as diffusion and annealing mechanisms are of fundamental and technological importance as these complexes are stable above room temperature. In Si the annealing of these E-centers occur at 413 K-473 K, depending on the dopant atom, while in Ge the annealing temperature is 20-40 K lower [22]. Markevich $et\ al.$ [23] utilized deep level transient spectroscopy (DLTS), capacitance-voltage (C-V) and current-voltage (I-V) techniques to study irradiated n-type oxygen lean Ge crystals doped with either P, As, Sb or Bi (N_{d}=10^{13}-10^{15} cm^{-3}). They argued that E-centers have three charge states in the band gap: double negative, single negative and neutral, each having a different activation energy for charge carrier emission depending on the impurity atom. Later Nylandsted Larsen and Mesli [24] reported on a third energy level in Sb doped irradiated Ge. According to Ref. [24], the (1+/0)- and (0/1-)-states are located below mid gap at E_{v}+0.10 eV and E_{v}+0.30 eV respectively and the (1-/2-)-state is in the upper half of the band-gap at E_{c}-0.30 eV.

Bulk Si has very poor optical properties due to the indirect band gap. However, when the size of the Si crystal is in the nanometer scale, this gap is direct. Thus, a strong quantum yield (QY) can be observed. [25] Reported values for QY varied from 10-70%. ($e.g.$ [26] and [27]). Unique optical properties and low toxicity make nanocrystals (NC) a very interesting material to be used in various applications. The possibility to use SiNC in LEDs [28,29], in bio-labeling [30] and in sensing applications [31] have yielded interesting results. Additionally, the insight gained from nanocrystals is certainly beneficial in microelectronics as the scale of the transistors is approaching the 10 nm node range.

2.3 Gallium antimonide

GaSb belongs to the III-V family of compound semiconductors. With a narrow and direct band gap it is considered to be suitable for devices requiring high mobility and high saturation velocity. In addition, its lattice parameter of $\sim$6.1 Å makes it a good candidate to be used as a substrate material for various compounds (see Ref. [32]). GaSb structures also have potential to be used in booster cells that improve the efficiency of pho-

tovoltaic devices [33]. Other potential application for GaSb is $e.g.$ laser diodes with low threshold voltages [34, 35].

As-grown GaSb is unintentionally p-type irrespectively of growth technique or conditions. Earlier studies have suggested that the formation of the acceptor can be related to V_{Ga} or Ga_{Sb}. However, the origin of the p-type conductivity of undoped GaSb is still under debate. In Publ. V we have applied positron annihilation spectroscopy to study native point defects and to identify the origin of p-type conductivity in bulk GaSb.

2.4 Diffusion

Diffusion of atoms in crystals can be divided into two main types: diffusion through interstitial sites and through lattice sites. In interstitial mediated diffusion the impurity atom can be dislodged from the lattice site into an interstitial position. The atom can then diffuse as an interstitial atom until a new lattice site is found [36, 37]. In vacancy mediated diffusion the impurity atom and a vacancy exhange positions. In substitutional lattice diffusion atoms diffuse by exhanging lattice positions with each other. This direct-exhange process is rather slow compared to the indirect diffusion via vacancy defects or interstitials.

The size of the impurity atoms has a large role in dictating the diffusion mechanism. Larger atoms need more space and favor diffusion via vacancy defects. Smaller atoms can move between the lattice atoms and prefer interstitial diffusion. It is also possible that a vacancy and an impurity atom diffuse through the lattice as a pair [17]. In Publ. IV it is suggested that a ring diffusion mechanism is responsible for the formation of vacancy-dopant complexes. In ring diffusion the electrostatic attraction keeps the complex together and allows the vacancy to move along the ring of the host atoms.

3. Positron annihilation spectroscopy

Positron annihilation spectroscopy is well suited for studying point defects in solids. The method is based on the implantation of positrons in the target material and the detection of the 511 keV γ quanta produced in the annihilation of positrons with electrons. Positrons, as positive particles, are sensitive to negatively charged and neutral vacancy defects. With PAS one is able to get information on the size of the vacancy defects, their concentration in the sample, charge states and the chemical surroundings around the defect. Positron annihilation spectroscopy is commonly used in two different modes in defect studies: Positron annihilation lifetime spectroscopy and Doppler broadening spectroscopy. In lifetime measurements the time difference between one of the two 511 keV photons and the 1.27 MeV photon emitted together with the positron in the β-decay of ^{22}Na is measured. The positron lifetime in the defect free lattice is shorter than in the vacancy, where the electron density is reduced. Doppler broadening measures the momentum distribution of the annihilating positron-electron pair by measuring the energies of the annihilation photons and is suitable for probing the chemical surroundings of the vacancy defects.

3.1 Positrons in solids

Positrons can be produced in several ways. In large scale facilities high intensity sources are used in nuclear reactors or particle accelerators. These sources, based on the pair production process, yield up to 10^{12} positrons per second. More common laboratory-scale sources use radioactive ^{22}Na isotopes with more modest positron yields of 10^9 positrons per second and with a half-life of 2.6 years.

The positron loses its energy rapidly in condensed matter reaching thermal energies in a few picoseconds [38,39]. After thermalization the positron

is in a Bloch like delocalized state in a periodic lattice. When the positron is trapped to $e.g.$ a vacancy defect it will transfer its energy and momentum to the crystal lattice. The positron trapping rate κ describes how fast positrons are trapped to a defect (D)

$$\kappa = \mu_{\mathrm{D}} c_{\mathrm{D}}. \tag{3.1}$$

Here, μ_{D} is the trapping coefficient (10^{15}-$10^{16}\mathrm{s}^{-1}$ at room temperature (RT)) [39]. The trapping coefficient depends on the defect and the host lattice. For positively charged traps the coefficient is small due to the Coulombic repulsion, thus positron trapping to positively charged vacancies is not observed. For negative vacancies the trapping coefficient is temperature dependent. At low temperatures 30-80 K the trapping coefficient has a $\mathrm{T}^{-1/2}$ dependence, due to phonon scattering. At temperatures 100-300 K the temperature dependence of the coefficient is much stronger ($\mathrm{T}^{-1.2}$) due to positron trapping through shallow Rydberg-like states [39]. The trapping coefficient for neutral traps is temperature independent. If the open volume of the negatively charged vacancy trap is increased by $e.g.$ removing an additional atom adjacent to the vacant lattice site, the trapping efficiency of the vacancy defect and the lifetime of the trapped positron increases. Negatively charged non-open volume defects, such as acceptor impurities, can trap positrons at shallow Rydberg-like states. The annihilation signal from these defects is similar to the defect-free lattice, due to the wide spatial extent of the positron wave function.

3.2 Positron lifetime spectroscopy

In positron lifetime measurements the time between the 1.27 MeV gamma photon emitted simultaneously with the positron and one of the photons emitted in the positron-electron annihilation is measured. These time differences are recorded in a histogram and thus a positron lifetime spectrum is created. The spectrum can be represented theoretically with the equation

$$n(t) = \sum_{\mathrm{i}} I_{\mathrm{i}} e^{-t/\tau_{\mathrm{i}}}. \tag{3.2}$$

Typically one million events are recorded in order to have good statistics. The experimental positron lifetime spectrum is a sum of exponentially decaying components convoluted with a Gaussian resolution function. τ_{i} is the positron lifetime in state i and t is the measured time difference. If

the sample does not have a detectable amount of vacancies, the spectrum has a single exponential component, and shows a linear behavior on a log scale. Each slope in the tail part of the spectrum corresponds to an annihilation state which has its own intensity and lifetime. Decomposition of the spectrum into several components is usually successful only if the lifetime components are well separated. Typically this is the case when $\frac{\tau_{i+1}}{\tau_i}$>1.3-1.5 [39]. Usually at most 3 lifetime components can be resolved reliably from a lifetime spectrum. If the positron trapping is in saturation, $i.e.$ all positrons are trapped to defects, or the concentration of trapping defects is too low ($\sim 10^{15}\mathrm{cm}^{-3}$) only one lifetime component can be fitted to the spectrum.

The most accurate quantity that can be obtained from the spectrum is the average positron lifetime:

$$\tau_{\mathrm{ave}} = \sum_{\mathrm{i}=1}^{N} I_{\mathrm{i}} \tau_{\mathrm{i}}, \tag{3.3}$$

where N is the number of lifetime components. The coefficients I_{i} are the intensities of each lifetime component τ_{i} in the spectrum. τ_{ave} corresponds to the center of mass of the lifetime spectrum and is therefore insensitive to the decomposition procedure. Whether the sample contains vacancy type defects or not, can be evaluated from τ_{ave}, which is higher in a sample with vacancy defects than in defect free bulk (218 ps for Si and 228 ps for Ge). With a proper setup and sufficient measurement time, it is possible to measure changes in τ_{ave} on the scale of 1 ps. If the positron trapping is dominated by a single vacancy defect and the trapping to these defects is not saturated, the decomposition of the lifetime spectrum yields two components. The longer lifetime components can be associated with the positron lifetime in the vacancy defect τ_2=τ_{D}. τ_1 corresponds to a modified bulk lifetime $\tau_1 = (\tau_{\mathrm{B}}^{-1} + \kappa)^{-1}$, where κ is the trapping rate. From the trapping rate one can estimate the defect concentration via Eq. 3.1.

Positron implantation of the unmoderated positrons can be described with the semi empirical stopping profile

$$p(x) = \alpha e^{-\alpha \mathrm{x}}, \tag{3.4}$$

where $\alpha = 16\frac{\rho}{E_{\mathrm{max}}^{1.4}}$, x is the penetration depth of the positron in the medium, ρ [g/cm^3] is the density of the sample and E_{max} [MeV] is the maximum energy of the emitted positron. [40]

Typically a ^{22}Na source is sandwiched between two identical samples. This packet is then placed between two fast scintillator detectors. In an

analog setup the pulse obtained from the detector is amplified and fed to a constant fraction discriminator which produces the start and stop timing pulses. When the 1.27 MeV start pulse is detected, the discriminator gives a signal to the time-to-amplitude converter. The RC circuit within the converter starts to charge up until the stop pulse is observed by the other detector. The charge stored in the converter is dependent on the charging time. This charge is then fed to a multichannel analyzer, which stores the time difference between the start- and stop-signals. In a digitalized setup, the data acquisition is handled by a circuit card.

3.3 Doppler broadening spectroscopy

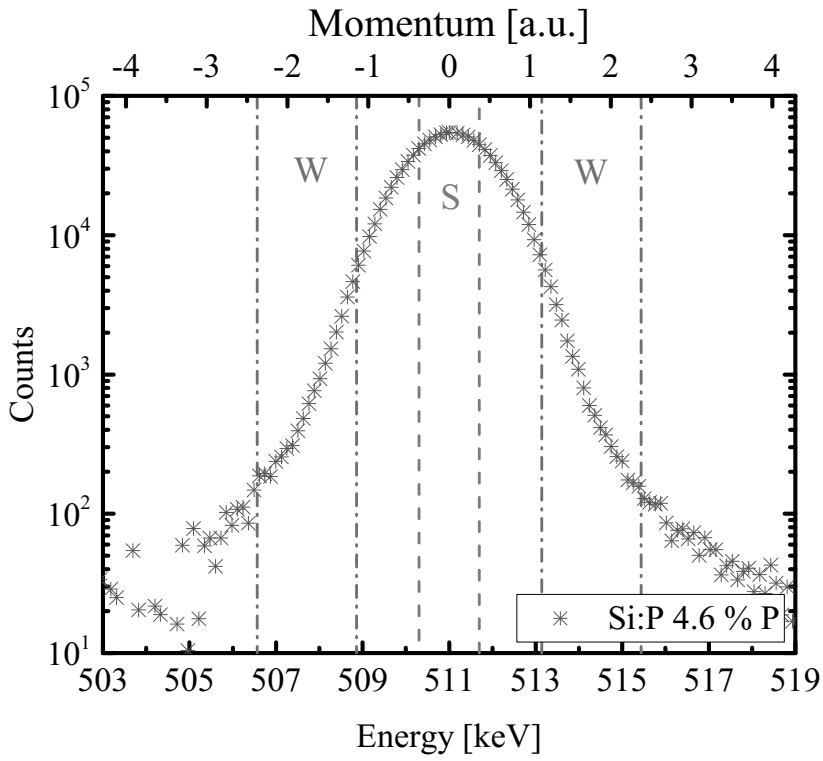

Figure 3.1. A background reduced Doppler spectrum. The S- and W-regions are shown as dashed vertical lines..

In positron Doppler broadening spectroscopy the energies of the photons emitted in the annihilation event of the positron and the electron are detected. In the annihilation two 511 keV gamma quanta are emitted approximately in opposite directions. The Doppler effect observed in the annihilation radiation is due to the annihilating positron-electron pair

acting as a moving source having a momentum component p_{pe} in the direction of the annihilation photon emission. The frequency of the photons is shifted due to the Doppler effect. This causes a shift in the energy of the photon described by $\Delta E = \frac{1}{2} p_{\mathrm{pe}} c$. Prior to annihilation the positrons are thermalized. Thus, in practice it is the momentum of the electron that is transferred to the two annihilation photons. In order to observe small energy shifts, high purity Ge detectors are used which have an energy resolution of $\sim$1.3 keV at 511 keV. The resulting Doppler broadened annihilation peak is studied by using line-shape parameters. These parameters are defined as ratios of distinctive areas of the peak to the total area of the peak. The low momentum parameter S (shape) describes the fraction positron annihilating with low momentum electrons, $i.e.$ close to the center of the peak. The W-parameter (wing) describes the fraction of positrons annihilating with high momentum electrons corresponding to the wings of the 511 keV line (see Fig. 3.1). The electron density is locally reduced when an atom is removed from a lattice site. When a positron is localized to such a defect it has a decreased chance to annihilate with core electrons compared to annihilation with valence electrons. This typically leads to a narrowing of the Doppler peak and consequently to an increase in the S-parameter and a decrease in the W-parameter.

Unlike in a lifetime setup, the positron implantation energy can be moderated in a Doppler broadening setup. The implantation profile for monoenergetic positrons can be described by the Makhovian implantation profile

$$p(x) = \frac{d}{dx} \mathrm{e}^{-(\frac{x}{x_0})^2}, \tag{3.5}$$

where x_0 is the position of the profile maximum. The mean stopping depth for positrons is $\tilde{x} = AE^r/\rho$ where A and r are empirical parameters, ρ is the mass density of the sample and E is the positron acceleration energy. Due to the asymmetrical shape of the profile the mean stopping depth is not equal to the maximum of the profile.

The benefit of being able to moderate the positron implantation energies is that it is possible to use positrons to probe vacancy defects in thin layered structures. In a slow positron beam setup fast positrons are moderated by letting them pass a thin tungsten foil which has a negative work function for positrons. The majority of the positrons either annihilate in this foil or pass it unmoderated. A small fraction of positrons thermalizes and diffuses to the surface of the foil and is spontaneously emitted. These positrons are then accelerated to the desired energy and driven to

the target with magnetic fields. The unmoderated positrons are deflected towards the walls of the beam line.

With a moderated positron beam it is not possible to record the positron lifetime. This would require the usage of a pulsed beam, where pulsing at a fixed frequency allows for the determination of the start timing pulse. More information on the pulsed positron beam can be found from Ref. [41] and references therein.

In a typical Doppler broadening experiment S- and W-parameters are measured and presented as a function of positron implantation energy. The measured parameters are superpositions of the parameters for the different annihilation states in the sample:

$$S = \sum_{\mathrm{i}} \eta_{\mathrm{i}} \, S_{\mathrm{i}}, \tag{3.6}$$

$$W = \sum_{\mathrm{i}} \eta_{\mathrm{i}} \, W_{\mathrm{i}}. \tag{3.7}$$

Here S_{i} and W_{i} are the S- and W-parameters of the state i and η_{i} is the annihilation fraction in state i. In this work typically the surface, a deposited layer and a substrate gives their own distinctive S- and W-parameters. Another way to present line-shape parameters is to draw the results in a (S, W)-plane which helps in annihilation state identification. The possible positron annihilation states in the sample could be $e.g.$ a surface state and a defect free bulk state. In such a case a straight line between the states is expected in the (S, W)-plane. A deviation from this linearity suggests that more than two positron trapping states are present. The strength of the trap can be evaluated from the plot by observing the slope of the curve in the SW-plane. In the case of a strong positron trap a sharp turning point in the intersection of the lines from the surface to trap state and from the trap state to bulk state is observed. This type of plot is used for data analysis in Publs. I, II and III.

In this thesis the majority of the Doppler broadening measurements are performed in two modes. In normal Doppler broadening mode, one HPGe detector is used to detect the energies of the emitted photons. For a sufficient statistical accuracy, 1×10^6 events are recorded for each spectrum. In 1D coincidence mode one high-purity (HP) Ge detector is used to measure the gamma emissions from the positron-electron annihilations and another detector is used as a gate. This type of setup reduces the background by one order of magnitude. In Publ. I the samples were measured in 2D coincidence mode where two HPGe detectors are used to detect both

photons from the annihilation event. The benefit of using 2D-coincidence is the improved resolution by a factor of $\sqrt{2}$. For a good statistical accuracy 15×10^6 annihilation events need to be detected.

3.4 Theoretical calculations

Various parameters related to positron-electron interactions in the lattice and in defect structures can be calculated via atomistic modeling. In this thesis, the modeling of the electronic structures was based on the two-component electron-positron formulations of DFT. The benefit of utilizing calculations is that the defect structures can be defined accurately. Thus, a very detailed picture on the positron interactions in the lattice could be in the optimal case obtained. Unfortunately, due to approximations needed to keep calculations feasible, the results of the modeling rarely match completely with the experimental results. Thus, mostly trends between the results on the different defect structures should be considered. In this section, the basics of the DFT calculations are given with the emphasis on the conceptual description. More detailed information on calculations can be found $e.g.$ in Refs. [42–47].

Two-component DFT calculations are based on the Kohn-Sham scheme in which a non-interacting system with positron and electron densities equal to those of the true interacting system are modeled using a total energy functional. The total energy functional of the system takes into account the classical interactions between the electron and the positron, the kinetic energies of the non-interacting particles and many-body corrections. Minimization of the functional with a fixed number of positrons and electrons leads to single particle equations from which the densities can be calculated. In practice, approximations are used when solving the densities. In a general case, the correct many-body interactions cannot be expressed accurately with electron density alone and their influence must be estimated. Effectively, every electron in the lattice is modeled as if moving in a homogeneous electron gas. Consequently the electron exchange and correlation energy density, which compensates for the lack of correct many-body interaction effects, depends only on the local electron density. This approximation is called local density approximation (LDA). Another commonly used approximation is the generalized gradient approximation (GGA) which also takes into account the density gradients around the electrons [44]. Unfortunately, these approximations tend to

underestimate the energy band gap. Thus, more advanced hybrid functional methods can be used [48–51] which corrects the band gap problem. In this case, however, the computational cost is much higher.

Once the electron and positron densities ($n_+(\mathbf{r})$ and $n_-(\mathbf{r})$) are solved, the positron annihilation rate and lifetime are calculated from

$$\lambda = \frac{1}{\tau} = \pi\, r_\mathrm{e}^2 c \int d\mathbf{r} n_+(\mathbf{r}) n_-(\mathbf{r}) \gamma(n_-(\mathbf{r})). \tag{3.8}$$

Here r_e is the classical electron radius, c is the speed of light and γ is a parametrized enhancement factor within LDA at the zero-positron-density limit, which takes into account the increased electron density near the positron due to the many-body interactions. The momentum distributions of an electron-positron pair is given by

$$\rho(\mathbf{p}) = \pi\, r_\mathrm{e}^2 c \sum_\mathrm{j} \gamma_\mathrm{j} \left| \int e^{-i\mathbf{p}\cdot\mathbf{r}} \psi_+(\mathbf{r}) \psi_\mathrm{j}(\mathbf{r}) \right|^2, \tag{3.9}$$

where the sum is taken over occupied electron states and γ_j is an enhancement factor depending on the electron states [39, 46]. In order to compare the calculations with experimental results, calculated distributions must be convoluted with a Gaussian to account for the detector resolution.

4. On interfaces and interface states in Si/SiO_2 structures

The research on nanocrystals has progressed rapidly during the last decade. In 2004, Klimov *et al.* discovered that SiNCs could convert single photons into more than one exciton [52]. Another benefit associated with the nanocrystals is that their energy sensitivity is dependent on the size of the nanocrystals. Thus, the absorption edge of the SiNC could be shifted towards the visible range of the Sun's spectrum allowing for a wider sunlight spectrum coverage. Unfortunately, despite the efforts, no such devices has yet been realized. Si nanostructures are also a very interesting material for optoelectronics, bio imaging and sensing applications, *e.g.* [28–31].

In this chapter the study on silicon nanocrystals embedded in a SiO_2 lattice is introduced. The study of interface defects in SiNC samples grown with RF magnetron sputtering are studied in Publ. I. A similar study but performed on samples grown with the PECVD method is perfomed in Publ. II.

4.1 Results and discussion

The structures of the PECVD grown and RF sputtered SiNC samples are shown in Fig 4.1. Each as-grown PECVD sample was subjected to one of the following heat treatments: 1h in 800 °C in N_2, 1h at 1150 °C in N_2, 1h at 1150 °C in N_2 and subsequent N_2+H_2 passivation at 500 °C for 1h. Three types of RF sputtered samples were measured with PAS: as-grown samples, samples annealed in N_2 at 1100 °C for 1h and samples annealed in N_2 at 1100 °C for 1h and subsequent N_2+H_2 passivation at 500 °C for 1h.

A slow positron beam was used to study the annihilation characteristics of the PECVD grown and RF sputtered sample sets. Doppler broadening

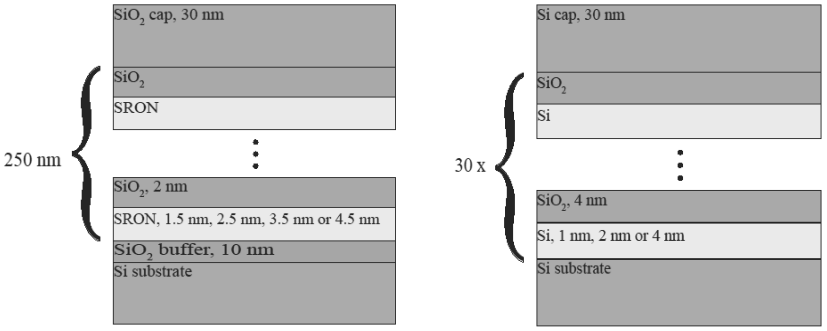

Figure 4.1. The structure of PECVD (left) and RF sputtered samples (right). In PECVD treated samples the layers consist of bilayers of Silicon Rich OxyNitride (SRON) and SiO_2 whereas in RF sputtered samples Si/SiO_2 layers were usedf.

measurements were performed at RT. Samples were also measured with PL at RT using a Si-CCD attached to a single grating monochromator and under excitation of a HeCd laser (3.8 eV line). All spectra were corrected for the spectral response of the setup.

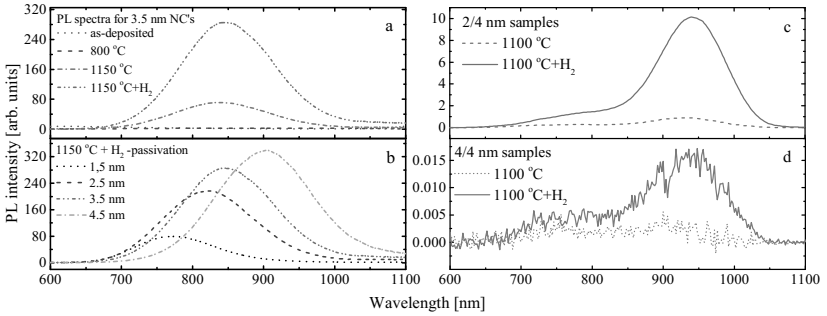

Figure 4.2. Photoluminescence intensities as a function of wavelength. Shown on the left are PL spectra from 3.5 nm SiNC samples after each production step (panel a) and from passivated samples having varying nanocrystal sizes (panel b). On the right PL spectra from RF sputtered samples with 2 nm (panel c) and 4 nm (panel d) Si layer.

In Fig. 4.2, panels a and b show the results from the PL measurements performed on the samples grown by PECVD. The PL spectra after the different heat treatments measured from the 3.5 nm samples are shown in panel a. An increase in PL signal was observed after the formation of NC. The passivation treatment further increased the PL intensity. This increase was explained with the compensation of dangling bond defects at the SiNC/SiO_2 interface. In panel b the spectra after the 1150°C+H_2 passivation step is shown. The increase in the PL intensity and the shift of the peak from 775 nm to 910 nm when the size of the NC grows from 1.5 nm to 4.5 nm is due to the changes in the band gap width in the NC.

The larger is the size of the nanocrystal, the smaller is the bandgap of the NC. This clearly indicates that the quantum confinement effect can be observed from the PL results. The PL results obtained from the RF sputtered samples (panels c and d) show that the PL signal is strongest in the 2 nm sample and visible but very weak in the 4 nm sample. The 1 nm sample produced no PL signal. Unlike in the PECVD samples the PL peak is positioned at the same wavelength (∼950 nm) regardless of the thickness of the superlayer and size of the NC. This indicates that the recombination of excitons do not occur directly over the band gap, instead the PL signal originates most likely from defects.

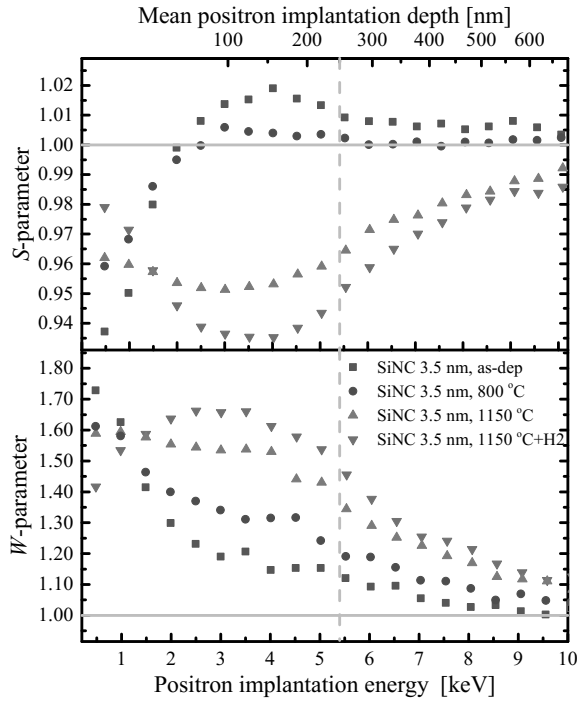

Figure 4.3. Normalized S- and W-parameters as a function of positron implantation energy. Full lines represent the corresponding parameters for bulk Si. The dashed line denotes the interface between the deposited layer and the substrate.

In Fig. 4.3 the normalized S- and W-parameters for the 3.5 nm sample grown with PECVD as a function of positron implantation energy are shown. Out of the samples measured with Doppler broadening spectroscopy the 3.5 nm sample was selected for the coincidence Doppler broadening spectroscopy measurements due to its PL characteristics. The results were normalized to the parameters from a defect free Si sample, S_{Si}=0.5515 and W_{Si}=0.0175. The deposited layer lies at a depth of 30-330

nm. The interface between the layer and the substrate is denoted as a vertical dashed line in the figure. The S-parameter for the as-deposited sample has a maximum at 3.5 keV. In terms of positron implantation depth this corresponds to $\sim$150 nm, $i.e.$ the positron implantation profile is centered in the layer. Heat treatment at 800 °C produces amorphous quantum dots in the sample and leads to a decrease in the S-parameter. In the heat treatment at 1150 °C crystalline nanodots are formed. In these samples the S-parameter is 5% lower compared to samples treated at 800 °C. The S-parameter is further reduced in the sample subjected to the passivation treatment. The (E,S)-graph shows a steep slope at 0.5 to 3.5 kV for the 800 °C and passivated sample and at 3.5 to 7.5 kV for sample treated at 1150 °C. This implies that the positron diffusion length is short $i.e.$ positrons are trapped very fast after thermalization. Clear maxima and minima in the S-parameter in as-deposited and in passivated samples indicate that the majority of the positrons is localized to a strong trap in the layer rather than annihilating in a delocalized state.

The positron S-parameter as a function of positron implantation energy for the samples grown with RF sputtering are presented in Publ I. The multilayer structure can be seen as a flat plateau at implantation energies 1-5 keV. As in the case of PECVD grown samples, the S-parameter for the heat treated RF sputtered samples exhibits a maximum which can be seen at 2 keV. This is almost negligible in the case of the 1 nm sample but is seen more clearly on 2 nm, 3 nm and 4 nm samples. The effect of passivation decreases the S-parameter in the layer, signaling a change in positron trapping. The results from the PAS measurements correlate well with the PL results; the PL signal from the 2 nm sample is the strongest whereas the PL signal from the 1 nm could not be observed.

Fig. 4.4 shows the (S,W)-plots for the PECVD grown samples. Three positron annihilation states can be distinguished in the as-deposited plot and are denoted as follows: surface (Sf), layer (L) and substrate (S). In the samples heated at 800°C a curvature (denoted by a dashed line) can be seen in the line between the layer state and the substrate state. This indicates the onset of positron annihilation at the interface between the amorphous NC and the surrounding matrix. The layer states in the samples with crystalline nanodots (panel c) are close to the Si/SiO_2 interface point reported earlier by Kauppinen $et\ al.$ [53]. The (S,W)-plot exhibits turning points at the intersection of the surface-layer- and the layer-bulk lines implying that the trap state is strong. Sharper turning points can

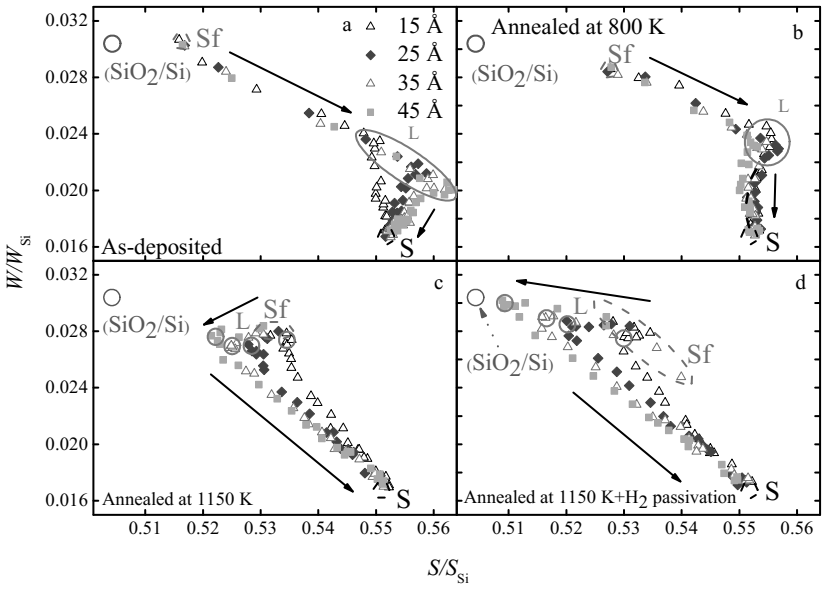

Figure 4.4. Normalized $S(W)$-plots of different SiNC sizes and and heat treatments. Arrows in the figure indicate the increasing positron implantation energy. Surface (Sf), substrate (S), layer (L) and SiO_2/Si interface point [53] are denoted in the plots.

be observed in the samples with bigger NC's while in the samples with smaller NC this turning point is more blunt. This is due to the area of the interface between NC and surrounding lattice. In the case of larger nanocrystal, a larger interface can be a strong trap for positrons, leading to a sharp turning point, whereas the surface of a smaller nanocrystal is not large enough to cause a sharp turning point in the (S,W) plane. After the passivation of the samples, the S- and W-parameters of the layer states were even closer to the interface state reported by Kauppinen *et al.* and all samples had sharp turning points. The passivation of the samples aims to compensate the dangling bond defects at the interface by partially filling them with hydrogen. The S-parameter in the passivated samples is lower compared to that of samples annealed at 1150°C. At the same time an increase can be seen in the PL spectra which indicates an increase in light conversion efficiency. In order to see how much the surrounding SiO_2 matrix modifies the S- and W- parameters, a Doppler broadening measurement was performed on a SiO_2 reference sample. Unlike in the SiNC samples the S-parameter for the SiO_2 decreased with each production step. Thus, the evolution of the line-shape parameters were clearly different in the SiNC samples compared to SiO_2, indicating that the changes seen in Fig. 4.4 are not due to changes in the SiO_2 lattice.

The Doppler results for the sample grown with RF sputtering revealed two unique positron states; the SiO_2/Si bulk interface state between substrate and the SiNC layer and an unknown state.

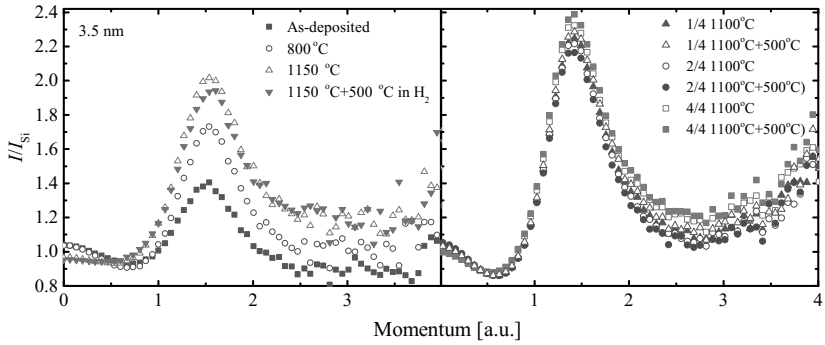

Figure 4.5. On the left ratio spectra from 3.5 nm sample measured after various production steps. Positrons were implanted with the energy of 3.5 keV. Dashed lines denotes the window used in determining the W-parameter value in the analysis. On the right ratio spectra from 1/4, 2/4 and 4/4 samples grown RF sputtering. Positrons were implanted with the energy of 2.0 keV. A defect free bulk Si sample was used as a reference. All measurements were performed at room temperature.

We performed 1D coincidence Doppler broadening measurements for the 3.5 nm PECVD samples whereas 2D coincidence setup was used for RF sputtered samples. To obtain the ratio curves, the positron-electron momentum distribution spectra from the samples were divided by the spectrum from a defect free Si sample. These ratio curves are presented in Fig. 4.5. The defining feature that all the ratio curves share is the large peak at $\sim$1.5 a.u. The as-deposited sample has the lowest peak whereas the largest peak is exhibited by the sample subjected to the 1150°C heat treatment. In the passivated samples this peak slightly decreased. The positron-electron momentum distribution spectra can be considered to be a sum of two parts: a high and a low momentum part. The low momentum part of the annihilation peak consists of events from positrons annihilating mainly with low momentum electrons, whereas positron annihilations with high momentum electrons gives rise to a broad tail part of the spectrum. The defect free Si spectrum has a kink at momenta where the high and low positron-electron momentum distributions coincide. In the samples with vacancy defects the lattice symmetry is disturbed. This is seen in the Doppler spectrum as a smoothening of the kink. Hence, a peak is observed in the ratio curve at the corresponding momentum. In earlier studies on p-type Si this type of a peak was related to positron trapping to vacancy-oxygen related traps [54, 55]. However, this peak is formed

due to a disturbance in the lattice symmetry. Thus it does not require the presence of oxygen in the lattice. Consequently, the peak seen in the ratio curve can have other origins than trapping to O-V type traps. The 2D Doppler ratio spectra for the RF sputtered samples are shown in Fig. 4.5 (right panel). The peaks at 1.5 a.u. have similar features as the peaks appearing in the ratio curves measured from PECVD samples. However, the intensities of the peaks for RF sputtered samples are higher and the variation of the peak height with the process step is smaller than in the PECVD samples. This indicates that in the RF sputtered samples the heat treatments have smaller influence on the positron-electron momentum distributions than in the case of PECVD samples. Nonetheless, in both sample sets a similar type of decrease in the peak height after the passivation treatment suggests that the positron annihilation occurs at the same type of interface defect in both sample sets.

5. Vacancy complexes in Si:P

By causing a controlled strain in a semiconductor lattice, a boost in the mobilities of charge carries can be obtained. In earlier studies it was suggested that the strain observed in Si:P films is due to clustering of P into stable Si_3P_4clusters [8]. In Publ. III, the formation of P-V complexes (as a possible alternative to Si_3P_4 clusters) and their influence on strain and conduction in Si:P films was studied with Rutherford Backscattering Spectrometry (RBS), Electron Spin Resonance (ESR) and PAS techniques. Also DFT calculations were performed to model several defect structures. This chapter extends the PAS part presented in Publ. III.

5.1 Doppler broadening measurements

Sample	P conc. [at.%]	Thickness [nm]
D2	1.8	47
D3	2.3	42
D8	4.6	60

Table 5.1. Si:P sample descriptions.

PAS was utilized to study vacancy defects in the Si:P layers. A summary of the samples is presented in Table 5.1. Fig. 5.1b and c show the S and W-parameters from the samples with different concentration of P before and after the HF etching. A spectrum measured from a defect free Si sample was used as a reference. Etching was done in order to remove the surface oxide on top of the thin Si:P layer. Fig. 5.1a shows the positron implantation profile for a few different acceleration energies. The effect of the oxide layer can be observed by comparing figures b and c. The steep slope at 0-2 keV in the $S(E)$-curve for the non-etched samples does not appear in the $S(E)$-curve for the etched samples. In the non-etched

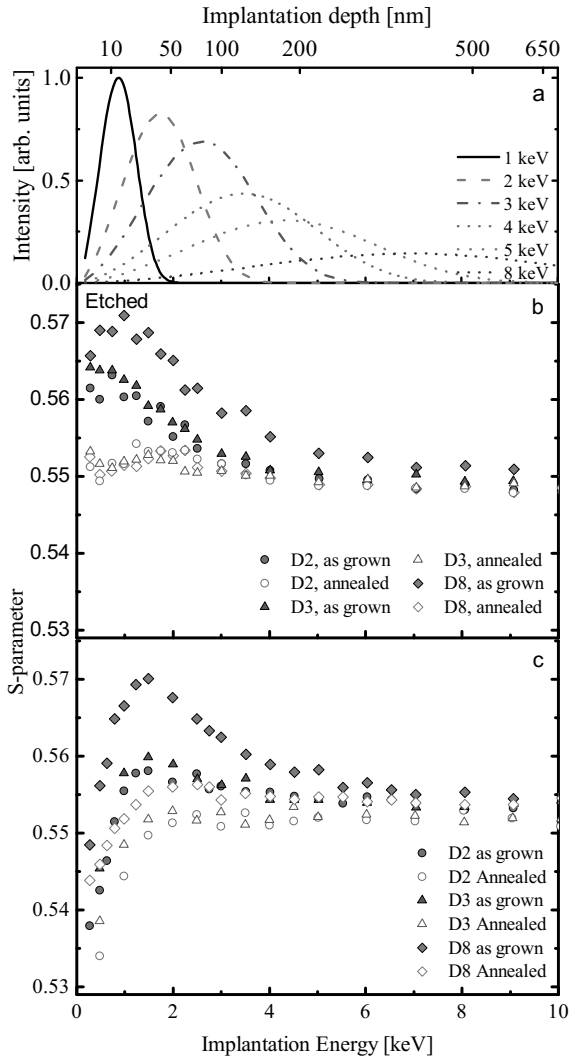

Figure 5.1. S parameters as a function of positron implantation energy after and before the etching (panels b and c). Panel a shows the positron implantation profiles for various energies. Values in the upper horizontal axis shows the mean implantation depth for positrons accelerated with the matching implantation energy (lower horizontal axis). The intensities of the implantation profiles are not in scale.

samples positrons annihilate in the native oxide on top of the Si:P layer yielding low S-parameter values. As a result, the measured S-parameter is lower than that of the non-etched sample (see Section 3.3). Due to the same reason, the maximum at 1.3 keV for etched samples containing 1.8 and 2.3 % P are more pronounced compared to those of non-etched samples. The effect of the oxide layer to positron trapping is weakest in the Si:P sample with the highest P concentration.

The maximum in S-parameter for the HF treated sample with a P concentration of 4.6 % indicates that positrons are trapped to a defect close to the surface. As the implantation profile for positrons implanted with low energy is very narrow (see Fig. 5.1a), it can be concluded that the S-parameter represents the positron annihilations in the Si:P layer. This same maximum in S-parameter appears also in the samples with a lesser amount of P, but is not as pronounced. In Fig. 5.2a the (S,W)-plots for

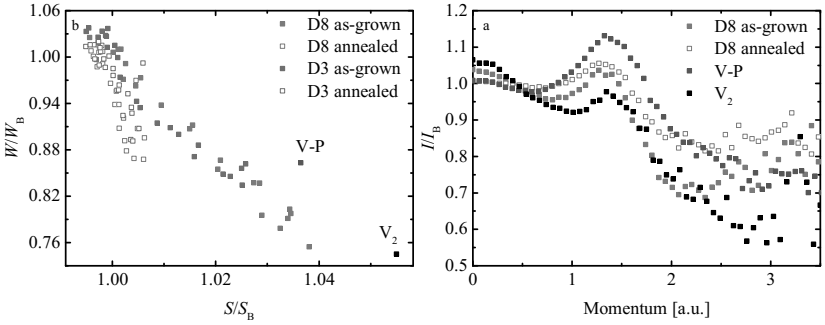

Figure 5.2. On the left (S, W)-plots for the samples containing 2.3% and 4.6% P are shown. On the right coincidence Doppler broadening ratio curves for the annealed and as-grown sample with 4.6% P are presented. Included are also results for the E-center (V-P) [17] and the divacancy in Si [56,57].

as-received and etched samples containing 2.3% and 4.6% P are shown together with the respective S- and W-parameters for an E-center (V-P) and a divacancy in silicon. [17, 56, 57]. The decrease of the S-parameter and increase of the W-parameter in the annealed samples indicates a reduction in the vacancy concentration (see Fig. 5.1).

5.2 Coincidence Doppler broadening measurements

The ratio curves from the 1D coincidence Doppler measurements for etched and non etched Si:P samples containing 4.6% P are presented in Fig. 5.2b. All the measured spectra were normalized to a defect free Si reference spectrum. For comparison, ratio curves for a divacancy in Si and the P-V complex in Si are shown [17, 56, 57]. In all samples a peak at $\sim$1.2 a.u. can be observed. The peaks of the as-received and annealed Si:P samples fall between the divacancy and P-V complex peaks with the peak of the annealed Si:P sample being closer to the P-V curve. In a study by Ranki *et al.* [17], it was shown that the addition of P atoms next to a Si vacancy decreases the intensity at high momenta. Thus, the coincidence results suggested that the dominating defect in the as-grown layers

is most likely a V-P_n complex. However, positrons trapping to divacancy sized defects was not ruled out.

6. Complex formation in highly doped bulk Ge

Germanium has been overshadowed by silicon in semiconductor devices. Only in recent years have the advancements in semiconductor technology permitted the manufacturing of novel Ge-based devices $e.g.$ hetero-bipolar transistors, high-mobility complementary metal-oxide-semiconductor devices and mid-infrared photodetectors. [14] In this chapter the formation of dopant complexes in Ge samples doped with As, P and Sb are studied with PAS.

6.1 Results and discussion

In this thesis highly P, As and Sb doped [P, As, Sb]$\approx 10^{19}$cm^{-3} Czochralski-grown Ge samples were studied with positron lifetime and Doppler broadening spectroscopies. Calculations of the positrons states and the annihilations in bulk Ge and defects were based on DFT.

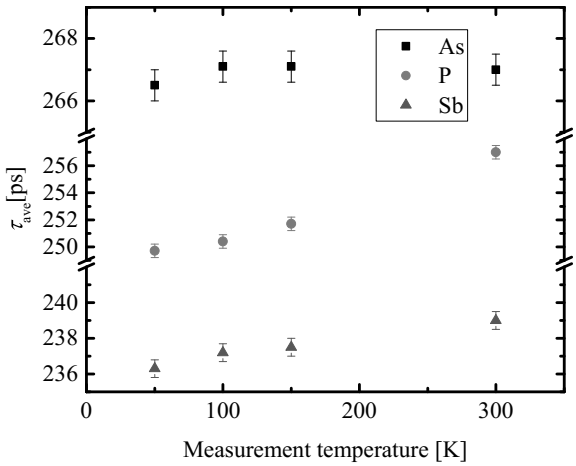

Figure 6.1. The average positron lifetimes in highly doped as-received Ge.

The positron lifetime results (see Fig. 6.1) revealed that the average life-

time τ_{ave} in Ge(As) and in Ge (P) was clearly longer than in Ge bulk. This indicated that positrons were probing vacancy defects. In both cases only one lifetime component could be fitted to the data. This suggested that the positron annihilation was either in saturation, where all positrons annihilate at one type of defect, or in a saturation-like state where all positrons annihilate at more than one type of defect.

Slotte $et\ al.$ reported earlier of a 272 ps lifetime component in Ge and associated this with the positron lifetime in a monovacancy [58]. Of the measured lifetimes the average positron lifetime in Ge(As) is closest to 272 ps. In addition, τ_{ave} is much lower than the lifetime component of 300-330 ps associated with the divacancy. [58, 59] Thus, the temperature independent 267 ps lifetime component was associated with the positron lifetime in a defect with an open volume of monovacancy size. In contrast to Ga(As) the average lifetime in the P doped Ge was temperature dependent; an increase in the temperature resulted in an increase in τ_{ave}. τ_{ave} in Sb doped Ge was only 4-5% higher than the positron lifetime in a defect free Ge lattice and exhibited a very weak temperature dependence. The small difference in average positron lifetimes implies that only a fraction of positrons annihilate in a localized state, $i.e.$ positron annihilation in Ge(Sb) is not in saturation. The average positron lifetime in Ge(As) was the longest lifetime measured in the samples. Thus, no defects with larger open volume, $e.g.$ divacancies, are introduced in amounts observable by PAS into the samples.

1D coincidence Doppler spectra were measured for each sample and normalized to bulk Ge. The resulting experimental ratios are shown in panel a in Fig. 6.2. A significant decrease in intensity at high momenta (p>1.5 a.u.) was seen in Ge(As) and in Ge(P). This is due to a reduced annihilation probability with the 3d electrons of Ge as these electrons give the largest contribution in the high momentum region of the ratio curve. The intensity of the ratio curve for the Ge(Sb) was close to unity.

Positron interactions in bulk Ge and in Ge defect complexes were modeled using LDA [44], and employing the projector augmented-wave (PAW) [60] method. The calculations were performed using a supercell consisting 216 atoms. In each modeled system the supercell contained 1-3 impurity atoms adjacent to a vacancy. These defect structures were relaxed, taking into account the repulsive forces of positrons on ions. In table 6.1 calculated positron lifetimes for different complex structures are presented and panel b in Fig. 6.2 shows the calculated ratio curves for

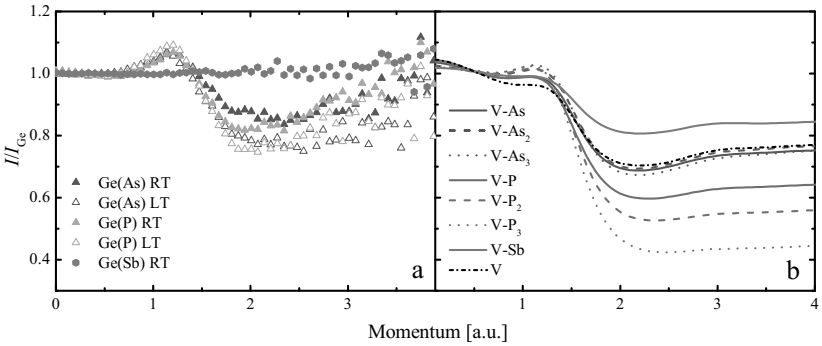

Figure 6.2. Experimental (panel a) and calculated (panel b) positron-electron momentum distribution ratios for Ge(As), Ge(P) and Ge(Sb).

	As	P	Sb
D_1	248	257	225
D_2	241	255	214
D_3	241	263	214
Ge bulk	213		

Table 6.1. Calculated average positron lifetimes. D_i indicates the number of dopant atoms around the vacancy.

each modeled system. A well known disadvantage of LDA is that it underestimates the energy band gap. In the case of Ge this effect is severe enough to close the gap, thus calculations cannot properly describe localized gap states. These aforementioned aspects will unavoidably bring some discrepancies between the calculated and measured data. Thus, rather than comparing results directly, similarities in trends between computational and experimental data should be compared. Furthermore, due to the reasons mentioned above the charge-state dependency of the positron lifetime is not considered. Instead, DFT calculations were performed for neutral defect centers.

Ranki *et al.* [17] studied complex formation and migration processes in highly n-doped Si. The dopant migration proceeds via the ring mechanism in which negatively charged vacancies form pairs with positively charged dopants. The electrostatic attraction keeps the complex together and allows the vacancy to move along the ring of Si atoms in the <110> plane. [61, 62] At the saddle point the vacancy has moved away from the dopant atom and is at the third nearest neighbour site. From there it can return to the dopant atom using a different route and thereby complete the migration step. Due to the similarities in atomic structures of Ge and

Si we proposed that the same mechanism applies to Ge. The concentration of vacancies is much smaller than the concentration of dopant atoms. Thus, it is more likely that a vacancy meets a dopant atom than another vacancy. Consequently, no divacancies are created in a high enough concentration. Furthermore, after the third dopant atom is attached to a complex, it is assumed to become immobile [17]. This occurs as a large fraction of vacancies are bound to complexes and cannot mediate the diffusion. Thus, the formation probability of bigger complexes than V-D_3 is very small.

Brotzmann *et al.* [63] studied diffusion of n-type dopants in Ge. For modeling the dopant diffusion they used the vacancy mechanism where singly positively charged substitutional dopants form complexes with doubly negatively charged vacancies. They noted that the size of the complex is dependent on the dopant concentration in the lattice. Consequently, the formation of larger complexes is more probable at high doping concentrations whereas smaller complexes are formed when concentration is lower. We proposed that the vacancy mechanism Brotzmann *et al.* used in their study is also valid with bigger complexes. This implies that the larger complexes can become neutral whereas smaller complexes can be negatively charged and thus more efficient positron traps.

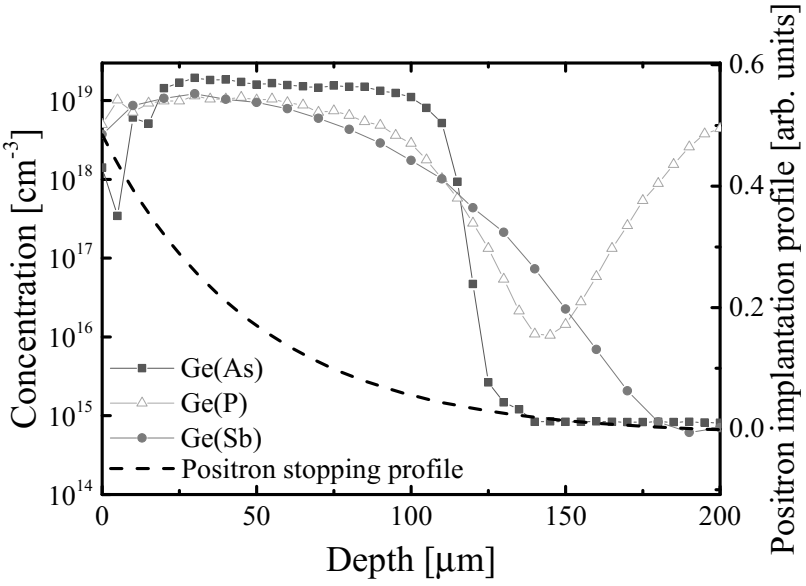

Figure 6.3. Dopant concentration for As, P and Sb (cm^{-3}) in Ge obtained from the spreading resistance measurements. The calculated positron implantation profile is shown by the black dashed line in arbitrary units. The sensitivity limit for the positron annihilation is $\sim 10^{15}$ cm^3 which is set to zero (see right axis).

The dopant concentration profiles measured for three dopant types have quite different shapes when it comes to the deep end edges of the profiles ($i.e.$ the diffusion tails of the profiles; see Fig. 6.3), due to different annealing temperatures. According to Fig. 6.3 the concentration profile of Ge(As) has a very abrupt edge at the deep end of the box shaped profile. Therefore, the formation probability of the small complexes ($i.e.$ the defect centers with one dopant atom next to a vacancy) is low. Thus, we proposed that the majority of positrons annihilates in complexes with a higher number of As atoms around the vacancy, $i.e.$ V-As_3 and that the positron annihilation was in saturation.

In Ge(P) the deep end tail is much broader than in Ge(As). This suggests, that in this region the smaller complex centers are more abundant and can have a larger influence on the positron trapping than in Ge(As). Thus, at higher temperatures trapping is dominated by larger complexes whereas at low temperatures trapping to smaller more negatively charged V-P_{1-2} complexes is more prevalent. DFT calculations performed on Ge(P) were consistent with the experimental results. They show that the positron lifetime is highest in a V-P_3 complex whereas lifetimes in V-P_1 and V-P_2 were lower and very close to one another.

As in Ge(As) and Ge(P) the concentration of different types of complexes in Ge(Sb) ($i.e.$ V-Sb_1, V-Sb_2 or V-Sb_3) is dependent on the dopant concentration. The doping concentration profile for Ge(Sb) decreases slowly with depth. In the Ge(P) sample V-$D_{1,2}$ complexes are more prevalent at the tail of the concentration profile whereas V-D_3 complexes are more abundant where the doping concentration is higher. Since the formation of V-Sb_{1-3} is similar to V-P_{1-3}, we proposed that the dominating defect in Ge(Sb) is the V-D_3 complex. The average positron lifetime in Ge(Sb) was close to the positron average lifetime in the Ge reference sample. This implied that a large fraction of the positrons annihilate in an unlocalized state. This can also be seen from Fig. 6.2a where the ratio for Ge(Sb) is very close to unity, $i.e.$ the chemical environment at the annihilation site of the positron and electron is similar to that in the defect free Ge. We suggested that two different processes can occur in the sample. If the V-Sb_3 complex is a weak positron trap, the positrons could de-trap from the vacancy center. Positron lifetime of a de-trapped positron is a mixture of positron lifetime in a trap and in a unlocalized state. In this case the lifetime components can have values too close to each other and thus it is not possible to resolve them. Another scenario is that positrons can an-

nihilate with smaller negatively charged V-Sb_1 centers which can affect the lifetime spectra even at relatively low concentrations. Due to this the average lifetime of the positrons is slightly higher than the positron lifetime in the reference sample. However, due to a low concentration of these complexes the intensity of the vacancy lifetime component is very low and thus the annihilations at these traps cannot be separated from the annihilations in a delocalized state. The DFT calculations performed for the system consisting of V-Sb_{1-3} centers suggests that positrons do not trap to defects with more than one Sb atom around the vacancy. This result was consistent with our positron trapping picture. Both the de-trapping from V-Sb_3 and the trapping to V-Sb_1 complexes alone could explain the results. However, it is likely that they occur simultaneously in the sample.

7. The source of p-type conductivity in undoped GaSb

Undoped GaSb is always p-type independent of its growth method. The origin of this p-type conductivity has been under debate. In this chapter n- and p-type GaSb samples are studied with positron annihilation spectroscopy. A strong influence of Ga_{Sb} on the positron lifetime is observed.

7.1 Results and discussion

The unintentionally p- and tellurium doped n-type ([Te]$\approx 6 \times 10^{17}\mathrm{cm}^{-3}$) samples were measured with a positron lifetime setup in the temperatures range of 30 K to 580 K. Results from these measurements are shown in Fig. 7.1

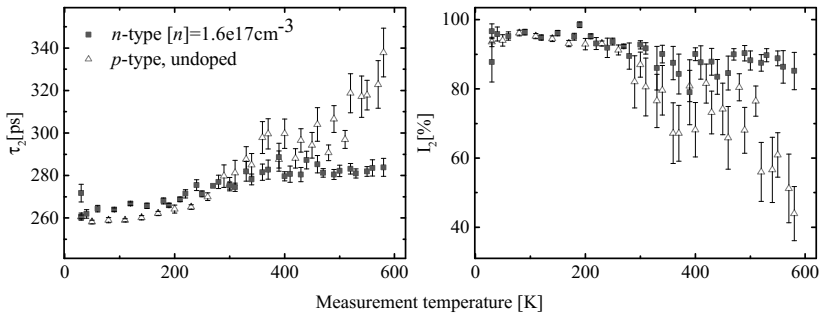

Figure 7.1. Lifetimes (left) and intensities (right) as a function of temperature obtained from the two-component model.

Lifetime analysis revealed that the two-component model, $i.e.$ in which two lifetime components are fitted to the lifetime data, was insufficient to fully describe the annihilations in the samples in the temperature range 30-330 K. In temperatures below 330 K the lifetime component τ_2 describing the positron annihilation in the defect decreased strongly. The intensity of this lifetime component was close to 100%. This was taken as a clue that there were more than one positron trap competing for the positrons.

The two trap model, worked relatively well above 330K where the intensity for τ_2 was $\sim$90% and τ_2 for n-type GaSb leveled out at τ_2=280$\pm$5 ps. This corresponds to a positron lifetime in a monovacancy size defect. In the unintentionally p-type GaSb (hereafter denoted as p-type GaSb) τ_2 forms a plateau with τ_2=295$\pm$10 ps in the temperature range of 360-510 K. This most likely corresponds to the same monovacancy defect as was observed in the n-type sample. We also attempted to fit three components to the spectra. Results from these fits were not physically reasonable and suggested that the lifetime components were too close to each other and thus the decomposition process was not successful.

Bracht *et al.* [64] studied Ga and Sb self diffusion in GaSb. Their investigations revealed that both Ga and Sb diffuse independently on their own sublattice. The Sb vacancy is unstable and cannot contribute to the Sb self diffusion whereas Ga vacancies are easily formed and they mediate the self diffusion of Ga atoms on the Ga sublattice. Consequently, we associated the observed monovacancies to V_{Ga}, which thus is the dominant vacancy defect in GaSb.

Negative ions form another group of traps in GaSb. The importance of the negative ions as positron trapping centers can be seen by observing Fig. 7.2, which shows the average lifetime as a function of measurement temperature. That the average positron lifetime decreases with decreasing temperature is in this case a fingerprint of negative non-open volume defects. Negative ions are competing with vacancy defects for the positrons [39, 40]. The positron binding energy in an ionic trap is typically very low $\sim$10-100 meV [39]. Thus, usually only at low temperatures ion-type states are able to trap efficiently. An increase in temperature increases the de-trapping rate from these shallow Rydberg like states and leads to a rapid decrease of positrons trapping to negative ions.

Another clue to the trapping efficiency of the ions could be observed from the measured momentum distribution ratios. Due to the lack of a proper reference sample (as-grown GaSb has a high native vacancy concentration) we used data measured from a p-type sample at 30 K as a reference. The positron lifetime was lowest at this temperature, indicating that the majority of the positrons do not annihilate at vacancy defects. The average positron lifetime in p-type GaSb increases 20 ps within the temperature interval 30 K-580 K. This suggests, that the annihilation environment should be quite different at 30 K compared to that at 580 K. However, this cannot be observed in the ratio curves for the n- and p-type

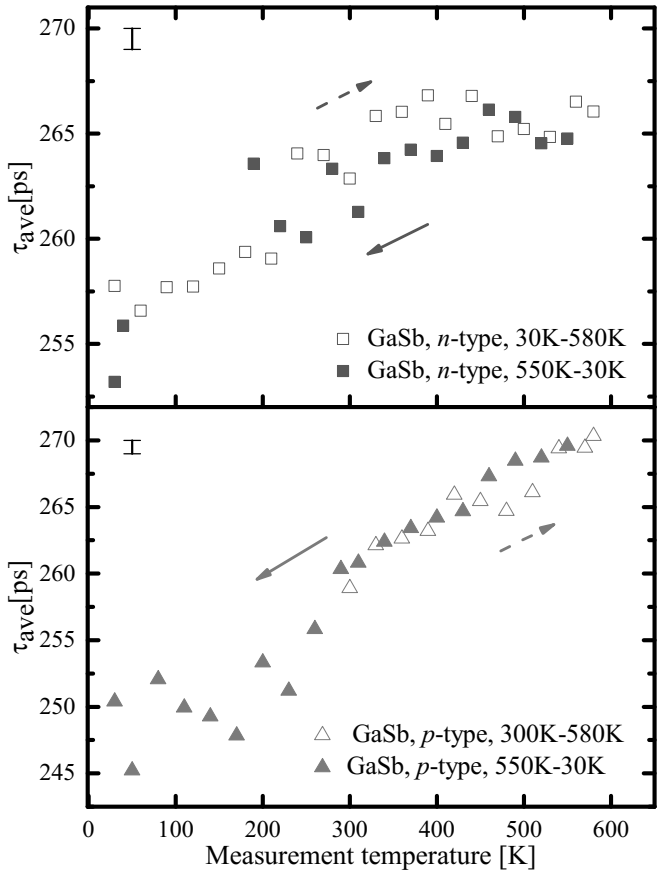

Figure 7.2. Positron average lifetime in p- and n-type GaSb. Open symbols indicate that the next measurement is done at a higher temperature than the preceding; the direction of the temperature change is represented by the dashed arrows. Closed symbols indicate that the next measurement is done at a lower temperature than the preceding; the direction of the temperature change is represented by the full arrows.

sample measured below 600 K. This shows that for the most part the annihilation environment resembles that of the reference (See Publ. 5, Fig 4). Small deviation from the reference can be observed above 1.2 a.u in the n-type sample measured at 600 K in which the intensity drops clearly below unity. The 3d electron shell of Ga atoms gives the largest contribution in the high momentum region of the spectrum. Removal of the Ga atom from its lattice site reduces the electron density locally, which is seen as a decrease in the intensity at high momenta.

As the ion-type traps are able to compete efficiently with the vacancy type traps, the concentrations of both trap types should be estimated. Concentrations of vacancy traps in the case of positrons trapping to one

defect can be estimated from [39]

$$c = \frac{\lambda_B}{N_{\mathrm{at}} \cdot \mu} \cdot \frac{\tau_{\mathrm{ave}} - \tau_{\mathrm{B}}}{\tau_{\mathrm{D}} - \tau_{\mathrm{ave}}}. \tag{7.1}$$

Here λ_B is the annihilation rate in the host lattice, N_{at} is the atom density, μ_{D} (units in at. s^{-1}) the defect specific trapping coefficient, τ_{ave} the average positron lifetime and τ_{B} and τ_{D} are the positron lifetimes in the bulk and in the defect states. Estimation of the Ga vacancy concentration was done using the data measured above RT, where the effect of negative ions is lowest. We obtained $[\mathrm{V_{Ga}}] \approx 4 \times 10^{16} \mathrm{cm}^{-3}$ for the n-type GaSb and $[\mathrm{V_{Ga}}] \approx 3 \times 10^{16} \mathrm{cm}^{-3}$ for the p-type GaSb. The concentrations for ion-type traps were estimated by comparing the trapping rates of Ga vacancies and ion-type traps [65]. We estimated the negative ion concentrations to be $1 \times 10^{17} \mathrm{cm}^{-3}$ and $2 \times 10^{17} \mathrm{cm}^{-3}$. for n- and p-type samples respectively. The concentration of negative ions exceeds the concentration of $\mathrm{V_{Ga}}$ by an order of magnitude. This makes them the dominant negatively charged defects in n- and p-type bulk GaSb.

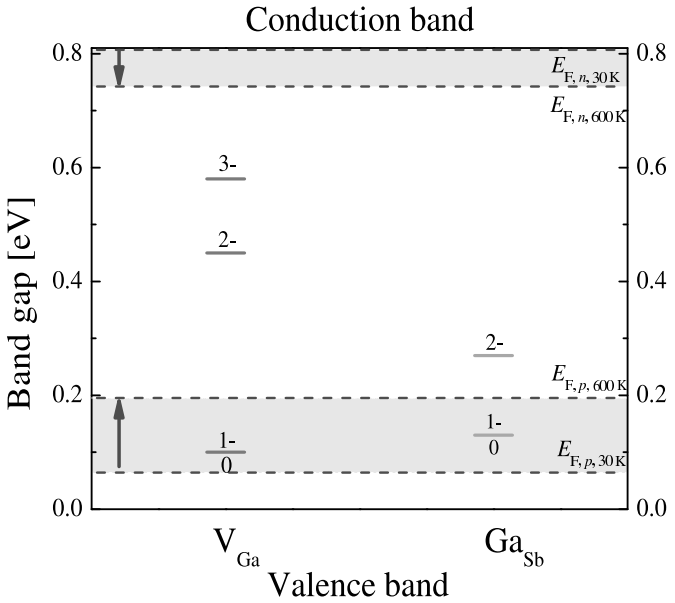

Figure 7.3. The GaSb band gap with the charge transition levels of $\mathrm{V_{Ga}}$ and $\mathrm{Ga_{Sb}}$ after Virkkala *et al.* [66]. The Fermi-level positions at 30 K and at 600 K in p- and n-type GaSb are represented with purple dashed lines. Yellow color indicate the area covered by the Fermi-level when the temperature is increased or decreased. The arrows indicate the direction of the Fermi-level movement when the temperature is increased.

Virkkala *et al.* calculated the formation energies and charge transition levels for various point defects in GaSb using the DFT framework [66]. They reported that the Ga antisite ($\mathrm{Ga_{Sb}}$) has the lowest formation en-

ergy of the acceptor-type defects. As our estimation shows that the ion-type trap is the most abundant defect type in n- and p-type GaSb, we associated these defects to Ga_{Sb}. At low temperatures τ_{ave} is close to the average positron lifetime in the p-type sample measured at 30 K, indicating that the majority of the positrons are trapped at negatively charged antisites. When the temperature increases, the trapping rate of positrons to the negative ions decreases. Consequently a larger fraction of positrons annihilate at negatively charged vacancy defects. Due to this, an increase is seen in τ_{ave} of the n-type sample at 30-300 K. The plateau above 300 K indicates that the positron trapping rate to antisites is low enough to make vacancy trapping more dominant.

We estimated the positions of the Fermi-levels by using the available electrical data. The position of the Fermi level at the highest and at the lowest measurement temperature was drawn in the charge transition level diagram (see Fig. 7.3). Comparison of the calculated charge transition levels and the position of the Fermi level suggested that in the n-type sample Ga_{Sb} is in the doubly negative charge state at all measurement temperatures. The positron average lifetime at low temperatures is close to the sample used as reference due to strong trapping efficiency of the negatively charged antisites.

In the p-type sample the Fermi-level was assumed to be pinned to the (0/1-)-level of the Ga_{Sb} at 30K due to the high antisite concentration. Unlike in n-type GaSb, an increase in temperature was not immediately followed by an increase in τ_{ave} in p-type GaSb. Instead, a plateau was observed at temperatures 30-200 K. This type of behavior occurs if V_{Ga} is in a neutral charge state and thus has a weaker trapping efficiency. An increase in average lifetime above 200 K is then due to a change in the charge state of V_{Ga} from 0 to 1-. Consequently, our experimental results suggested that the (0/1-) level of Ga_{Sb} is closer to the valence band than the (0/1-)-level of V_{Ga}. As the temperature is increased τ_{ave} continues to rise in linear fashion suggesting that no additional changes in the charge state of ions or vacancies occur and that the trapping to the antisites is significant even at higher temperatures.

Thus, we concluded that V_{Ga} is the dominating vacancy defect in both samples. However, the behavior of the average positron lifetime in both p- and n-type GaSb indicates that negative ions as trapping center for positrons compete with the Ga vacancies. Ga antisites in a negative charge state are nearly an order of magnitude more abundant compared

to that of Ga vacancies and dominate the positron annihilation at low temperatures. Hence, we concluded that Ga antisites are the major cause for p-type conductivity in bulk GaSb.

8. Summary

In this work positron annihilation spectroscopy is used to study point defects in elemental and compound semiconductors. Point defects can be introduced to the material, $e.g.$ during the growth or in the post-growth processes. Upon the formation, they can create new energy levels in the band gap of a semiconductor, which may have a detrimental effect on the electrical and optical properties of the material. Due to this, it is of a paramount importance that the properties of the defects are well known. The ability to control the formation of the defects in the material is a requirement which will grow in importance in the future as the microelectronic devices reach the 10 nm node range.

In Publs. I and II positron annihilation spectroscopy and photoluminescence is used to study silicon nanocrystals embedded within silica. In the samples deposited with RF sputtering the PL intensity and the S-parameter exhibit a behaviour which suggests that both signals originate from the same source, $i.e.$ from the interface between the nanocrystals and the surrounding silica matrix. In the samples grown with PECVD the quantum confinement effect could be observed. This indicates that the PL originates from the nanocrystals whereas analysis on the line-shape parameters revealed that the positrons annihilate at the SiNC/SiO_2 interface. The passivation of the samples results in a further decrease in the S-parameter. Furthermore, the introduction of H_2 into SiNC resulted in an increase in the PL signal. The decrease of the S-parameter and the increase of the PL signal suggested that the positron trap at the interface does not contribute to a significant extent to the exciton recombination in the nanocrystals.

Epitaxially grown Si:P films were studied in Publ III. A lattice strain is induced into highly P doped Si due to the formation of defect structures. Earlier reports suggested that the cause for the strain are Si_3P_4 clusters.

However, neither theoretical nor experimental proof were given for their existence. The coincidence Doppler broadening measurements suggested that the dominating defect in the as-grown layers is most likely a V-P_n complex, although positrons trapping to divacancy sized defects was not ruled out.

In Publ. IV the complex formation in highly As, P and Sb doped Ge is studied. High dopant concentration was achieved by diffusion. Vacancies and dopant atoms form complex centers consisting of a monovacancy and one to three dopant atoms. Combined results from the Doppler broadening, positron lifetime, DFT and spreading resistance measurements indicate that above RT positron trapping is dominated by the complexes with more than one dopant atom around the vacancy. At low temperatures, positron trapping to smaller complexes is more pronounced. In the case of As and P doped Ge the positron trapping was found to be in saturation or in a saturation-like state, whereas in Sb doped Ge a large fraction of positrons do not get trapped to complexes prior to annihilation.

Finally, in Publ. V, the positron annihilation spectroscopy results on GaSb are presented. As-grown GaSb is always p-type regardless of its growth method. Doppler broadening spectroscopy and positron lifetime measurements on unintentionally p-type and Te doped n-type GaSb revealed that two traps compete for positrons, the gallium vacancy and the gallium antisite. At low temperatures negatively charged gallium antisites dominate the trapping, whereas at higher temperatures the probability for positron to be trapped to Ga vacancies increases. Estimations on defect concentrations indicated that Ga antisites are nearly an order of magnitude more abundant compared to that of Ga vacancies.

References

[1] T. D. Veal, L. Piper, S. Jollands, B. Bennett, P. H. Jefferson, P. A. Thomas, C. F. McConville, B. Murdin, L. Buckle, G. Smith, and T. Ashley, Appl. Phys. Lett. **87**, 132101 (2005).

[2] P. H. Jefferson, T. D. Veal, L. Piper, B. Bennett, C. F. McConville, B. Murdin, L. Buckle, G. Smith, and T. Ashley, Appl. Phys. Lett. **89**, 111921 (2006).

[3] A. Belabbes, M. Ferhata, and A. Zaouib, Appl. Phys. Lett. **88**, 152109 (2006).

[4] D. Wang, S. Svensson, L. Shterengas, G. Belenky, C. Kim, I. Vurgaftman, and J. Meyer, J. Appl. Phys. **105**, 014904 (2009).

[5] K. Weeks, S. Thomas, P. Dholabhai, and J. Adams, Thin Solid Films **520**, 3158 (2012).

[6] P. Verheyen, V. Machkaoutsan, M. Bauer, D. Weeks, C. Kerner, F. Clemente, H. Bender, D. Shamiryan, R. Loo, T. Hoffmann, P. Absil, S. Biesemans, and S. G. Thomas, Elec. Dev. Lett. **29**, 1206 (2008).

[7] G. Eneman, D. Brunco, L. Witters, B. Vincent, P. Favia, A. Hikavyy, A. De Keersgieter, J. Mitard, R. Loo, A. Veloso, O. Richard, H. Bender, S. Lee, M. Van Dal, N. Kabir, W. Vandervorst, M. Caymax, N. Horiguchi, N. Collaert, and A. Thean, in *Elec. Dev. Meet.*, IEEE (IEEE, International, 2012), pp. 6–5.

[8] Z. Ye, S. Chopra, R. Lapena, Y. Kim, and S. Kuppurao, ECS Trans. **50**, 1007 (2013).

[9] E. Haller, Mater. Sci. Semicond. Process. **9**, 408 (2006).

[10] F. Schäffler, Semicond. Sci. Tech. **12**, 1515 (1997).

[11] S. E. Thompson, M. Armstrong, C. Auth, S. Cea, R. Chau, G. Glass, T. Hoffman, J. Klaus, Z. Ma, B. Mcintyre, A. Murthy, B. Obradovic, L. Shifren, S. Sivakumar, S. Tyagi, T. Ghani, K. Mistry, M. Bohr, and Y. El-Mansy, Electron Dev. Lett **25**, 191 (2004).

[12] S. Verdonckt-Vandebroek, E. F. Crabbe, B. S. Meyerson, D. L. Harame, P. J. Restle, J. M. Stork, and J. B. Johnson, Trans. Elec. Dev. **41**, 90 (1994).

[13] M. L. Lee, E. A. Fitzgerald, M. T. Bulsara, M. T. Currie, and A. Lochtefeld, J. Appl. Phys. **97**, 011101 (2005).

[14] K. Brunner, Rep. Prog. Phys. **65**, 27 (2002).

[15] A. N. Larsen, A. Mesli, K. B. Nielsen, H. K. Nielsen, L. Dobaczewski, J. Adey, R. Jones, D. Palmer, P. Briddon, and S. Öberg, Phys. Rev. Lett. **97**, 106402 (2006).

[16] S. Hu, Mater. Sci. Eng. R-Rep. **13**, 105 (1994).

[17] V. Ranki, A. Pelli, and K. Saarinen, Phys. Rev. B **69**, 115205 (2004).

[18] G. Watkins and J. Corbett, Phys. Rev. **134**, A1359 (1964).

[19] S. Brotherton and P. Bradley, J. Appl. Phys. **53**, 5720 (1982).

[20] V. Markevich, A. Peaker, V. Litvinov, V. Emtsev, and L. Murin, J. Appl. Phys. **95**, 4078 (2004).

[21] A. Chroneos and H. Bracht, Appl. Phys. Rev. **1**, 011301 (2014).

[22] A. Peaker, V. Markevich, F. Auret, L. Dobaczewski, and N. Abrosimov, J. Phys. Condens. Matter **17**, S2293 (2005).

[23] V. Markevich, I. Hawkins, A. Peaker, K. Emtsev, V. Emtsev, V. Litvinov, L. Murin, and L. Dobaczewski, Phys. Rev. B **70**, 235213 (2004).

[24] A. N. Larsen and A. Mesli, Physica B **401**, 85 (2007).

[25] K. Dohnalová, A. N. Poddubny, A. A. Prokofiev, W. D. De Boer, C. P. Umesh, J. M. Paulusse, H. Zuilhof, and T. Gregorkiewicz, Light: Sci. Appl. **2**, e47 (2013).

[26] J. Valenta, M. Greben, S. Gutsch, D. Hiller, and M. Zacharias, Appl. Phys. Lett. **105**, 243107 (2014).

[27] F. Sangghaleh, I. Sychugov, Z. Yang, J. G. Veinot, and J. Linnros, ACS nano **9**, 7097 (2015).

[28] R. J. Anthony, K.-Y. Cheng, Z. C. Holman, R. J. Holmes, and U. R. Kortshagen, Nano Lett. **12**, 2822 (2012).

[29] F. Maier-Flaig, J. Rinck, M. Stephan, T. Bocksrocker, M. Bruns, C. Kubel, A. K. Powell, G. A. Ozin, and U. Lemmer, Nano letters **13**, 475 (2013).

[30] B. F. McVey and R. D. Tilley, Accounts Chem. Res. **47**, 3045 (2014).

[31] A. Nguyen, C. M. Gonzalez, R. Sinelnikov, W. Newman, S. Sun, R. Lockwood, J. G. Veinot, and A. Meldrum, Nanotechnology **27**, 105501 (2016).

[32] P. Dutta, H. Bhat, and V. Kumar, J. Appl. Phys. **81**, 5821 (1997).

[33] J. Benner, T. Coutts, and D. Ginley, Technical report, American Institutes of Physics, New York, NY (United States) (unpublished).

[34] T. Kagawa and G. Motosugi, Jpn. J. Appl. Phys. **20**, 597 (1981).

[35] M. Morosini, J. L. Herrera-Perez, M. Loural, A. Zuben, A. Silveira, and N. Patel, J. Quantum Electron. **29**, 2103 (1993).

[36] P. M. Fahey, P. Griffin, and J. Plummer, Rev. Mod. Phys. **61**, 289 (1989).

[37] N. Cowern and C. Rafferty, MRS Bull. **25**, 39 (2000).

[38] M. J. Puska and R. M. Nieminen, Rev. Mod. Phys. **66**, 841 (1994).

[39] F. Tuomisto and I. Makkonen, Rev. Mod. Phys. **85**, 1583 (2013).

[40] K. Saarinen, P. Hautojärvi, and C. Corbel, Semiconduct. Semimet. **51**, 209 (1998).

[41] F. Reurings, Ph.D thesis (2010) .

[42] E. Boroński and R. M. Nieminen, Phys. Rev. B **34**, 3820 (1986).

[43] G. Kresse and J. Furthmüller, Comp. Mater. Sci. **6**, 15 (1996).

[44] J. P. Perdew and A. Zunger, Phys. Rev. B **23**, 5048 (1981).

[45] G. Kresse and D. Joubert, Phys. Rev. B **59**, 1758 (1999).

[46] I. Makkonen, M. Hakala, and M. J. Puska, Phys. Rev. B **73**, 035103 (2006).

[47] I. Makkonen, M. Hakala, and M. J. Puska, J. Phys. Chem. Solids **66**, 1128 (2005).

[48] A. D. Becke, J. Chem. Phys. **98**, 1372 (1993).

[49] J. P. Perdew, M. Ernzerhof, and K. Burke, J. Chem. Phys. **105**, 9982 (1996).

[50] C. Adamo and V. Barone, J. Chem. Phys. **110**, 6158 (1999).

[51] J. Heyd, G. E. Scuseria, and M. Ernzerhof, J. Chem. Phys. **118**, 8207 (2003).

[52] R. D. Schaller and V. I. Klimov, Phys. Rev. Lett. **92**, 186601 (2004).

[53] H. Kauppinen, C. Corbel, L. Liszkay, T. Laine, J. Oila, K. Saarinen, P. Hautojärvi, M. Barthe, and G. Blondiaux, J. Phys. Condens. Matter **9**, 10595 (1997).

[54] R. Brusa, W. Deng, G. Karwasz, A. Zecca, and D. Pliszka, App. Phys. Lett. **79**, 1492 (2001).

[55] A. Kruseman, H. Schut, A. Van Veen, and M. Fujinami, Nucl. Instrum. Meth. B **148**, 294 (1999).

[56] H. Kauppinen, C. Corbel, J. Nissilä, K. Saarinen, and P. Hautojärvi, Phys. Rev. B **57**, 12911 (1998).

[57] K. Saarinen and V. Ranki, J. Phys. Condens. Matter **15**, S2791 (2003).

[58] J. Slotte, S. Kilpeläinen, F. Tuomisto, J. Räisänen, and A. N. Larsen, Phys. Rev. B **83**, 235212 (2011).

[59] K. Kuitunen, F. Tuomisto, J. Slotte, and I. Capan, Phys. Rev. B **78**, 033202 (2008).

[60] P. E. Blöchl, Phys. Rev. B **50**, 17953 (1994).

[61] S. T. Pantelides, Phys. Rev. Lett. **57**, 2979 (1986).

[62] M. Ramamoorthy and S. T. Pantelides, Phys. Rev. Lett. **76**, 4753 (1996).

[63] S. Brotzmann and H. Bracht, J. Appl. Phys. **103**, (2008).

[64] H. Bracht, S. Nicols, W. Walukiewicz, J. P. Silveira, F. Briones, and E. Haller, Nature **408**, 69 (2000).

[65] F. Tuomisto, V. Ranki, D. C. Look, and G. C. Farlow, Phys. Rev. B **76**, 165207 (2007).

[66] V. Virkkala, V. Havu, F. Tuomisto, and M. Puska, Phys. Rev. B **86**, 144101 (2012).

Aalto-DD 223/2016

ISBN 978-952-60-7092-6 (printed)
ISBN 978-952-60-7089-6 (pdf)
ISSN-L 1799-4934
ISSN 1799-4934 (printed)
ISSN 1799-4942 (pdf)

Aalto University
School of Science
Department of Applied Physics
www.aalto.fi

BUSINESS + ECONOMY

ART + DESIGN + ARCHITECTURE

SCIENCE + TECHNOLOGY

CROSSOVER

DOCTORAL DISSERTATIONS